*buildings*

MDPI

*Article*

# Lateral Effects of Jet Grouting on Surrounding Soil and Circular Diaphragm Walls

**Yu Yao [1,*], Xuefei Shi [1] and Dongdong Han [2]**

[1] Bridge Engineering Discipline, Tongji University, Shanghai 200092, China
[2] CCCC Highway Bridges National Engineering Research Center Co., Ltd., Beijing 100011, China
* Correspondence: 2080039@tongji.edu.cn

**Abstract:** The installation of high-pressure jet grout piles induces significant lateral soil displacement, which can adversely affect nearby structures, such as diaphragm walls. Based on field tests, this study systematically analyzes the lateral displacement of soil caused by two distinct grouting techniques: the intelligent sensing super jet pile (SJT) technique and the Rodin jet pile (RJP) technique. Experimental results show that the SJT technique induces less disturbance to surrounding soil, with a maximum lateral displacement of approximately 6 mm at the closest inclinometer and an influence range limited to about 4 m. A theoretical model, based on passive pile theory, was developed to predict the lateral deflection of diaphragm walls due to adjacent jet grouting. Using a finite difference algorithm, bending moments on the walls were calculated and compared to measured data, showing a consistent correlation between predictions and observations. These findings are crucial for the design and construction of jet grout piles near sensitive structures, ensuring the safety and reliability of soil improvement practices and underground engineering.

**Keywords:** jet grout piles; soil improvement; lateral displacement; diaphragm wall; passive pile; deflection differential equation



**Citation:** Yao, Y.; Shi, X.; Han, D. Lateral Effects of Jet Grouting on Surrounding Soil and Circular Diaphragm Walls. *Buildings* **2024**, *14*, 3587. https://doi.org/10.3390/buildings14113587

Academic Editor: Fabrizio Gara

Received: 16 October 2024
Revised: 6 November 2024
Accepted: 7 November 2024
Published: 12 November 2024



## 1. Introduction

As cities expand and infrastructure projects increase in scale, urban underground space is becoming increasingly congested, complicating underground engineering efforts [1,2]. This congestion leads to more frequent interactions between construction activities, such as adjacent construction and undercrossing projects, which heighten concerns about the safety of underground structures [3,4]. Engineering activities such as construction loading, pit excavation, and pile driving can negatively impact nearby structures, leading to increased internal forces, deformation, and cracking. These effects compromise structural integrity and may result in catastrophic failures [5,6]. Notable incidents include the displacement of bridge piers due to subgrade filling of a highway in Lianyungang [7], and the collapse of the Nicoll Highway in Singapore during the MRT Circle Line construction in 2004, which claimed four lives [8]. These cases highlight the need for soil improvement techniques that enhance soil strength and deformation resistance while minimizing adverse impacts on surrounding structures.

High-pressure jet grouting is one of the most widely used and effective soil improvement techniques. This method involves injecting high-pressure cement slurry into the soil to create high-strength grout columns, which enhance load-bearing capacity and soil impermeability [9–11]. Due to its small construction footprint, low vibration, and minimal noise, jet grouting is ideal for projects subject to strict environmental and deformation controls, making it especially valuable in urban settings. However, jet grouting can also induce considerable ground disturbances, including ground deformation and surface heave, particularly in soft soil regions [12,13]. Grouting pressures reaching tens of megapascals, combined with the injection of large grout volumes, compress surrounding soil,

causing ground displacement that may affect nearby underground pipelines, walls, and buildings [14,15].

The potential impacts of jet grouting on the surrounding environment, particularly on diaphragm walls, have prompted extensive research [16–19]. These studies have employed various methods, including field observations, numerical simulations, and semi-theoretical and semi-empirical approaches. Field observation methods allow for the assessment of jet grouting disturbance patterns, enabling the development of empirical prediction formulas [20–22]. However, these findings are often specific to certain ground conditions, limiting their general applicability across diverse projects. For example, Fontanella et al. [21] noted that jet grouting within retaining structures of excavation sites can cause significant outward displacement of diaphragm walls, whereas the excavation process typically induces inward deformation. Wong et al. [22] reported that while diaphragm walls are effective in limiting displacements caused by jet grouting, the grouting process can generate bending moments in the walls that exceed 1000 kN·m/m. Numerical simulations allow for comparisons with field monitoring data, yet their practical application in engineering is often hindered by the complexity of input parameters. Feizi et al. [23] used numerical modeling to study the effects of grout pressure and flow rate on surrounding ground conditions, while Dong et al. [24] analyzed the impact of jet grouting on diaphragm walls, finding that it induces substantial lateral movements and bending moments. Semi-theoretical and semi-empirical methods, such as the cavity expansion theory in an infinite soil mass, have also been applied to characterize the jet grouting process [18,25]. However, these approaches typically overlook the presence of nearby structures, limiting their predictive accuracy. Despite extensive monitoring and simulation efforts, theoretical research remains limited, especially regarding the detailed mechanisms of soil–structure interaction during grouting. This gap highlights the urgent need for models that can more accurately capture the complex interactions between soil movements caused by grouting and the responses of adjacent structures.

The lateral displacement imposed on diaphragm walls due to jet grouting can be considered as a "passive pile problem" [26–29], where the load on the structure arises from soil movement rather than external forces directly acting on the wall itself. In this context, the diaphragm wall passively resists the soil displacement. Soil movement is the primary driver in passive pile problems, and it can be analyzed using methods like the two-stage analysis approach [30–32]. This approach evaluates the lateral effects of soil on the structure by first determining the free displacement field of the soil under external loads and then applying this displacement to the passive piles. Considerable research has been conducted on passive pile issues [33–36]. For instance, Zhang et al. [37] derived mathematical expressions for passive pile behavior by establishing control equations for pile–soil interaction, while Hu et al. [38] utilized $p$-$\delta$ and $p$-$y$ curves to simulate the pile–soil interaction, presenting an elastoplastic solution. Additionally, Zhao et al. [39] used numerical simulations to explore the effects of soil–structure interaction on passive pile behavior under different loading conditions, providing valuable insights into deformation patterns and load distribution.

In summary, the lateral effects of jet grouting on diaphragm walls have become a significant concern that requires careful control. Current studies lack effective methods for evaluating and predicting this impact before design and construction. Additionally, the interactions between jet grout piles, soil, and structures remain insufficiently understood, creating challenges for engineering practice. In the case of the south anchorage of the North Channel Bridge of the Zhangjinggao Yangtze River Bridge, the design involves installing jet grout piles after constructing circular diaphragm walls. This paper investigates the soil displacement induced by jet grouting and proposes a method to assess its impact on diaphragm walls.

## 2. Background

### *2.1. Project Overview*

The Zhangjinggao Yangtze River Bridge, located about 28 km downstream of the Jiangyin Bridge and 16 km upstream of the Hutong Bridge, connects Suzhou, Taizhou, and Nantong (see Figure 1). This project starts from the G40 Shanghai–Shaanxi Expressway and ends at the S82 Port Expressway, spanning a total length of about 29.8 km. It is divided into three parts: the cross-river bridge and the south and north approach lines; the river-crossing section comprises the north approach bridge, north channel bridge, middle approach bridge, south channel bridge, and south approach bridge; and the south and north channel bridges feature a double-tower, two-span suspension system with spans of 2230 + 717 m and a double-tower, single-span suspension system with a main span of 1208 m, respectively. Diaphragm wall foundations are employed for the foundations of the south and north anchorages of the south channel bridge and the south anchorage of the north channel bridge, with soil improvement to enhance the bearing capacity and impermeability of the bearing layer [40]. For the south and north channel bridge towers, bored pile group foundations are employed, incorporating post-grouting techniques at the pile tips to enhance bearing capacity and reduce settlement.

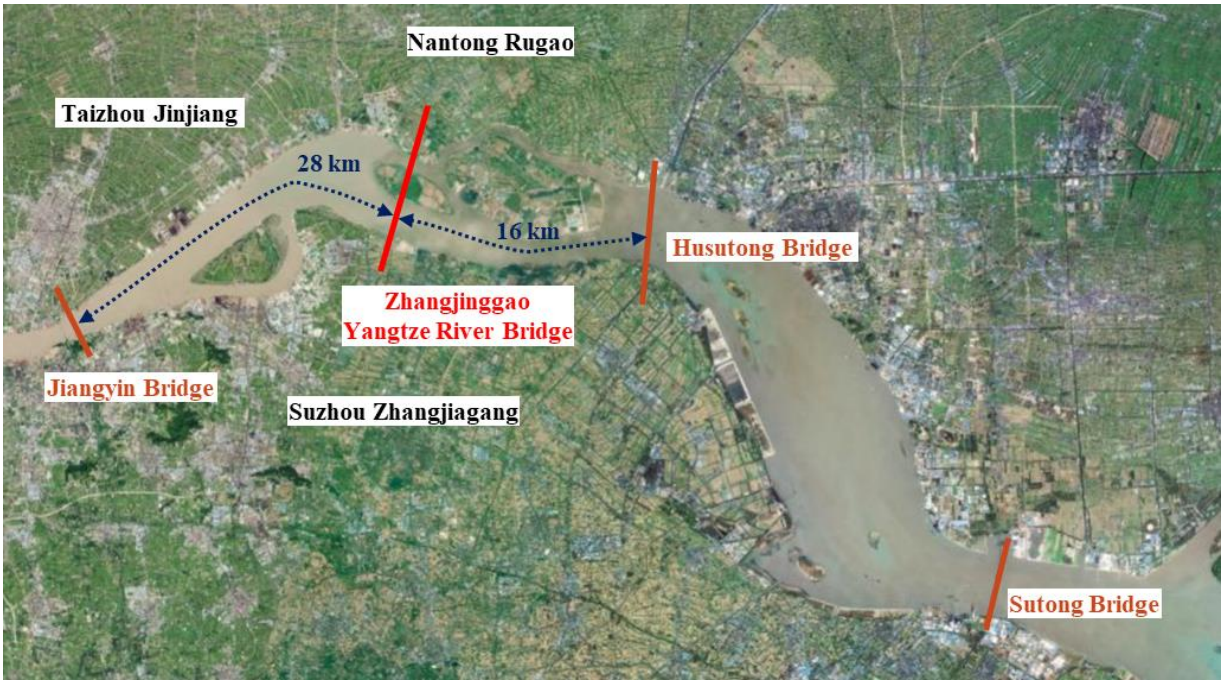


**Figure 1.** Location of Zhangjinggao Yangtze River Bridge.

### *2.2. Geological Conditions*

This study focuses on the foundation of the south anchorage of the North Channel Bridge, located on an alluvial island in the river. The strata primarily predominantly of Quaternary alluvial silt clay, with localized layers of silty sand. The upper strata range from loose to slightly dense, the middle strata range from slightly dense to moderately dense, and the lower strata are dense. The Quaternary cover layer is notably thick, with bedrock buried deeper than 120 m. As shown in Figure 2 and Table 1, the typical geological profile indicates that the weak overburden mainly comprises silty clay, characterized by low strength, low friction coefficient, poor plasticity, high compressibility, and a thickness ranging from 43.8 to 50.5 m. The sand layers, starting from level $⑦_5$ and below, are confined aquifers with a high water head, buried 1.6 to 3.25 m below the surface.

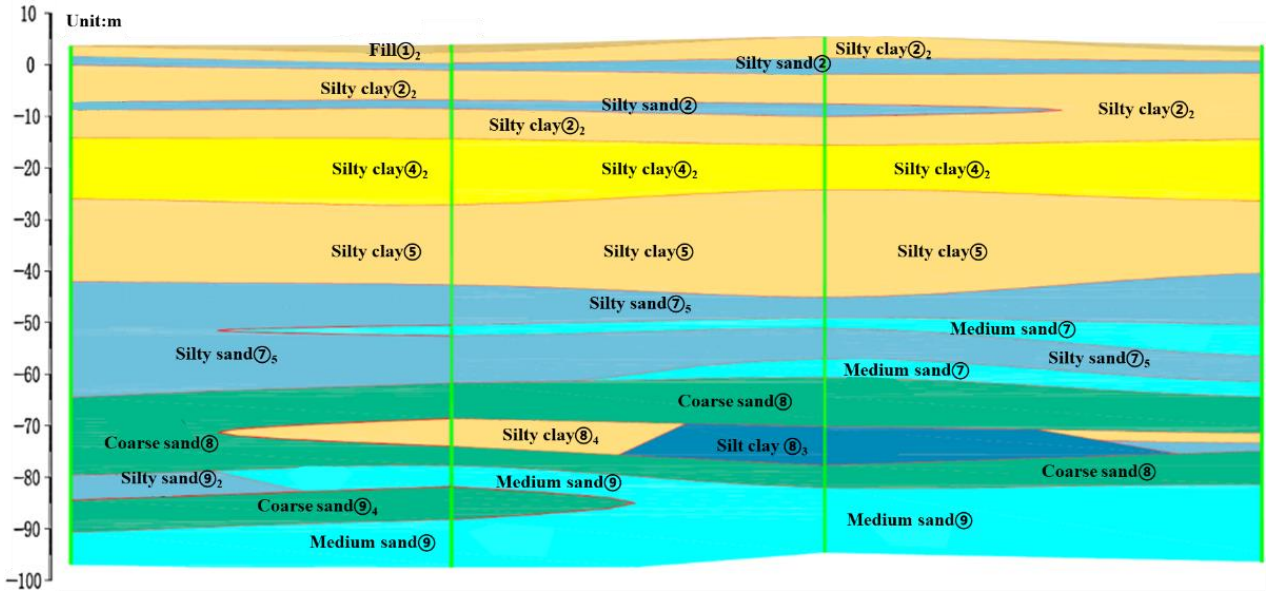


**Figure 2.** Geological profile of the south anchorage of the North Channel Bridge.

**Table 1.** Soil profiles at the project site.

| Layer | $\gamma$ (kN/m³) | $w$ (%) | $c$ (kPa) | $\varphi$ (°) | $E_s$ (MPa) | SPT ($N$) |
|---|---|---|---|---|---|---|
| ② Silt sand | 19 | 26 | 3.1 | 27.9 | 10.81 | 6 |
| $②_2$ Silty Clay | 18.4 | 34 | 12.2 | 6.9 | 4.25 | 6 |
| $④_2$ Silty Clay | 18.2 | 33 | 12 | 8 | 3.97 | 10 |
| ⑤ Silty Clay | 18.3 | 31 | 14 | 8.2 | 4.35 | 15 |
| $⑦_5$ Silty Sand | 19.7 | 18 | 3.3 | 29 | 12.36 | >50 |
| ⑦ Medium Sand | 19.8 | 18 | 4 | 28.3 | 14.01 | 47 |
| ⑧ Coarse Sand | 20.3 | 11 | 3 | 28.5 | 13.08 | >50 |

### *2.3. Anchorage Design*

Based on the geological conditions and the overall design of the anchorage, as shown in Figure 3, the foundation adopts circular diaphragm walls with an outer diameter of 90 m and a thickness of 1.5 m, along with an annular reinforced concrete inner lining support structure. The foundation is 21 m high, with a 0.3 m thick plain concrete pad underneath, and the excavation depth of the pit is 21.3 m. The foundation includes a 7 m thick top slab, a 7 m thick bottom slab, and a 7 m high concrete core. For the uniformity of stress distribution at the base, 32 empty chambers of 6 m × 6 m are set in the front half of the foundation core. Below the foundation is a 27.5 m thick artificially treated ground, located in the dense silty sand layer $⑦_5$. Jet grouting was applied to improve an approximately 6000 m$^2$ circular area within the diaphragm wall. A total of 2497 jet grout piles were installed, each 2.5 m in diameter with 1.8 m spacing and 0.7 m overlap.

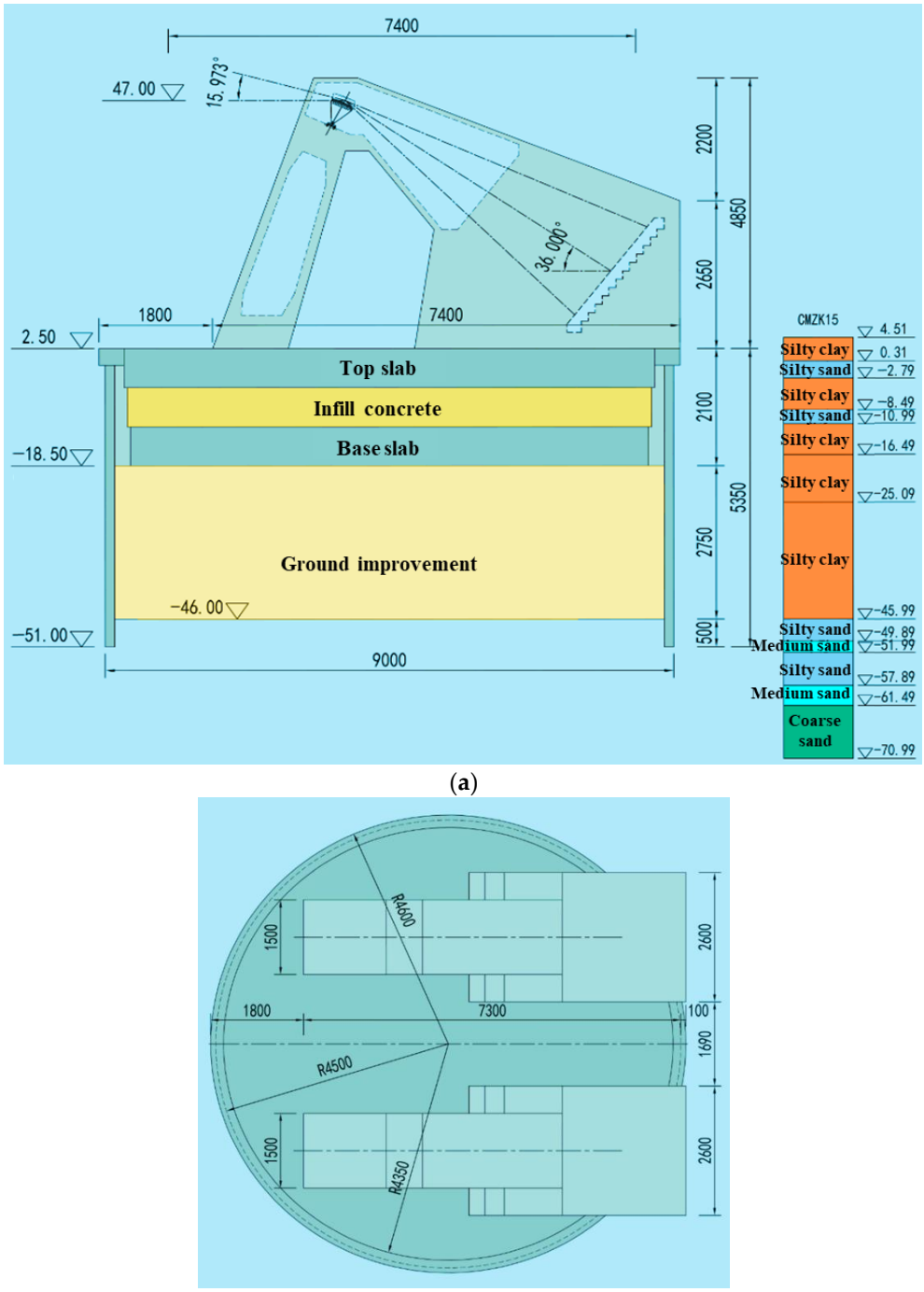


(**a**)




(**b**)

**Figure 3.** Design of the south anchorage of the North Channel Bridge. (**a**) Section.(**b**) Plan layout.

## 3. Lateral Displacement of Soil Induced by Jet Grouting

A field test was conducted to investigate free soil displacement induced by jet grouting. The experiment included two groups, each involving the installation of five jet grout piles labeled sequentially from 1# to 5#, as shown in Figure 4. Each pile had a diameter of 2.5 m, with an overlap of 0.5 to 0.7 m between adjacent piles, and extended to depths between 27 m and 56 m. Different construction techniques were used in the two groups: Group A employed the Intelligent Sensing Super Jet Pile (SJT) technique, while Group B used the Rodin Jet Pile (RJP) technique. The SJT method is an improved version of the RJP method. By integrating advanced sensors and intelligent algorithms, the SJT technique enables real-time adjustments of construction parameters, supporting quality control and automation

during grouting. Furthermore, its use of a larger pre-drilling hole diameter helps to reduce lateral effects on surrounding soil, making it a more adaptive and controlled approach.

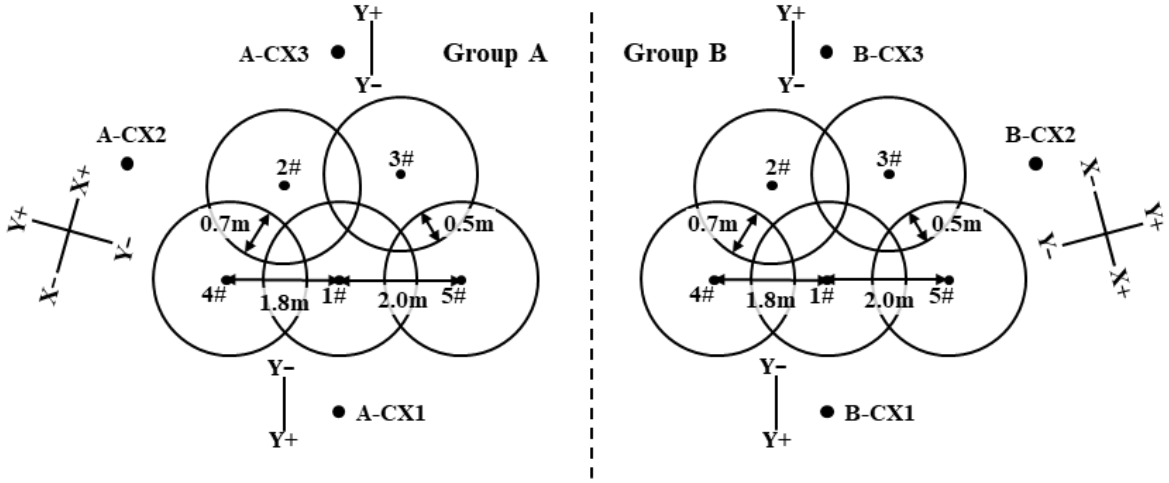


**Figure 4.** Layout of piles and inclinometers.

### *3.1. Monitoring of Lateral Displacement*

Inclinometers were used to monitor the lateral soil displacement, with their layout and orientation shown in Figure 4. Six inclinometers, each 56 m long, were positioned 1.5 m from the jet grout piles: three for Group A (labeled A-CX1, A-CX2, A-CX3) and three for Group B (labeled B-CX1, B-CX2, B-CX3). In Figure 4, the Y direction represents radial displacement, the X direction represents tangential displacement, and Y+ indicates displacement along the jetting direction. The inclinometer has an accuracy of ±0.05% of full scale, with a total system accuracy of ±3 mm over a 30 m range.

This paper focuses on soil displacement in the Y direction within the depth range of 27 to 56 m. Figure 5 illustrates soil displacement resulting from the SJT technique, where suffixes 1# to 5# denote inclinometer data recorded after the installation of piles 1# to 5#. Figure 6 shows the corresponding soil displacement induced by the RJP technique, allowing for a direct comparison between the two methods.

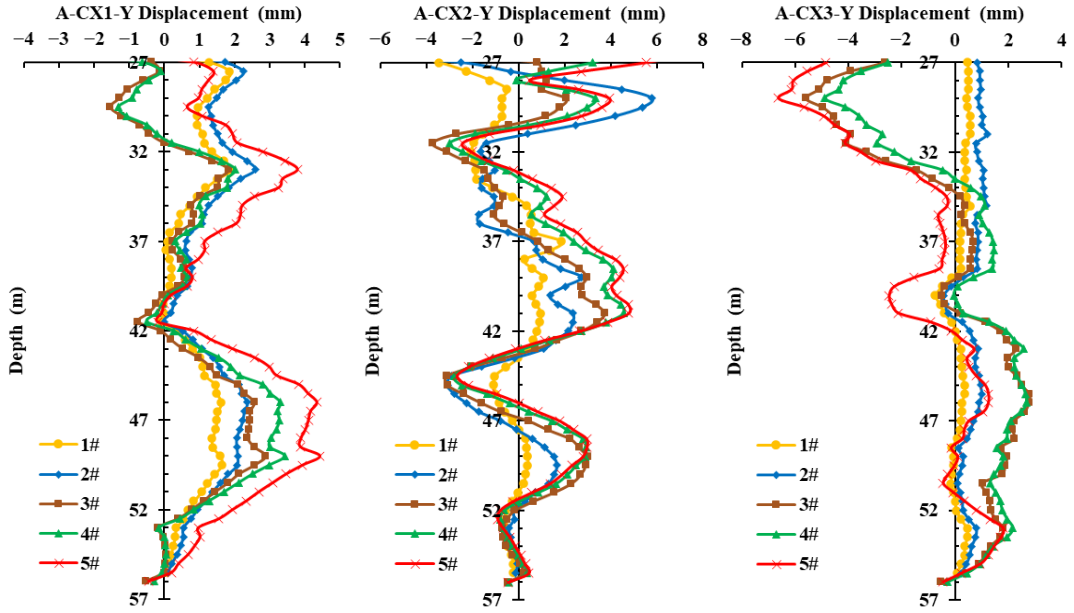


**Figure 5.** Y-direction displacement of inclinometers in Group A.

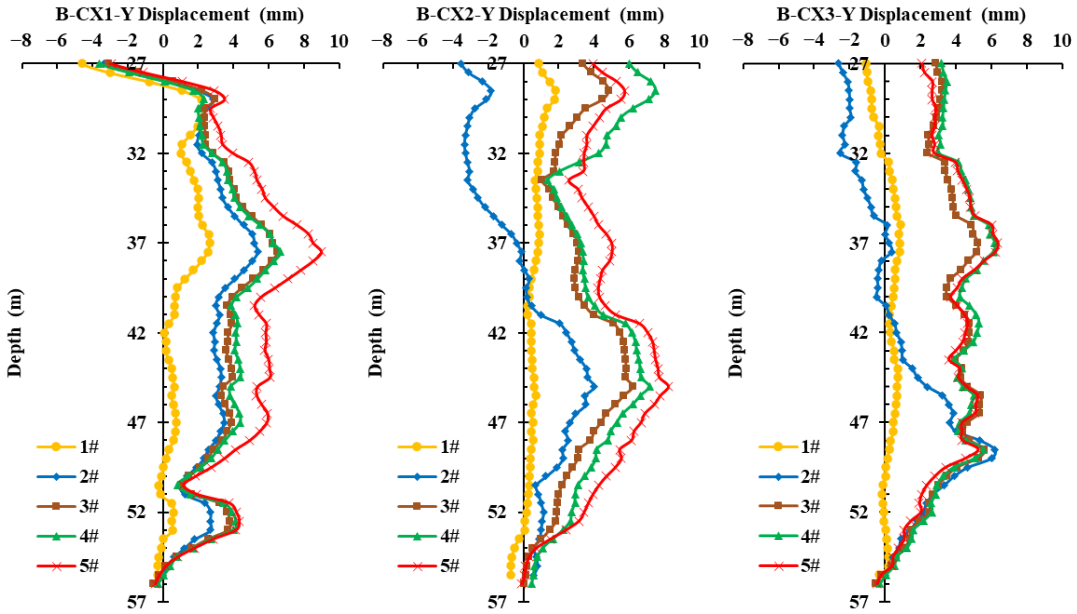


**Figure 6.** Y-direction displacement of inclinometers in Group B.

### *3.2. Analysis of Final Lateral Displacement*

After the construction of the jet grout piles, the lateral soil displacement for both Group A and Group B was monitored every 1–2 days until stabilization. Figure 7 compares the final lateral displacement in the Y direction for both groups. The maximum lateral displacements at measurement points CX1, CX2, and CX3 in Group A are approximately 6 mm, 5.5 mm, and 2.0 mm, respectively, whereas for Group B, they are around 8.5 mm, 9 mm, and 9.5 mm. These results indicate that the lateral displacement for Group A (SJT) is slightly lower than that for Group B (RJP). This reduction in or even reversal of displacement in Group A can be attributed to the SJT technique's real-time monitoring and adaptive adjustment of construction parameters, along with a slightly larger pre-drilled hole, which helps to minimize lateral pressure on the surrounding soil.

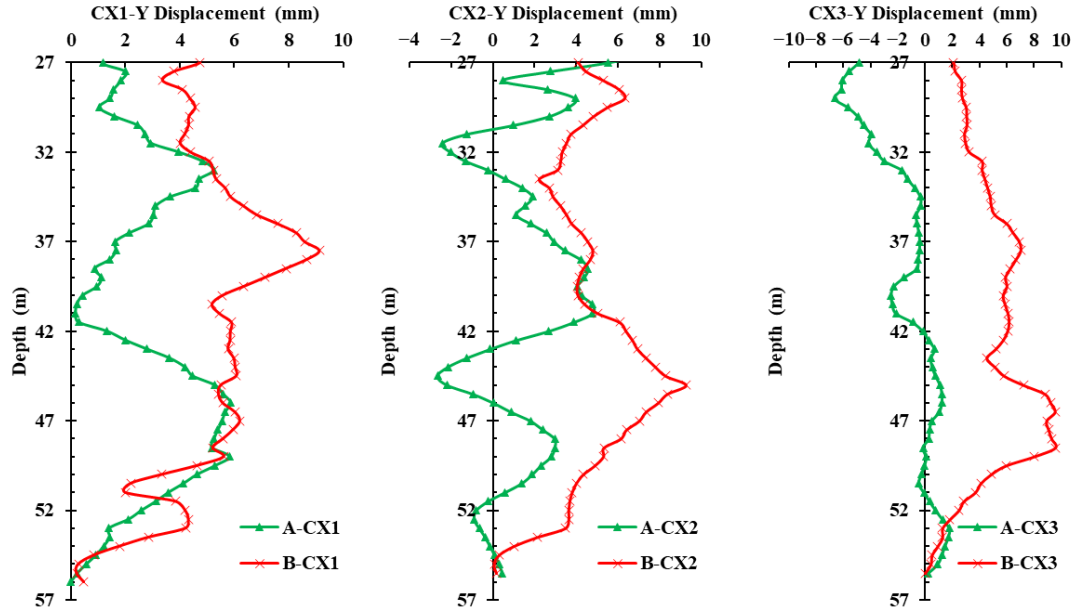


**Figure 7.** Comparison of Y-direction displacement between Group A and B.

### *3.3. Analysis of Grouting Impact Range*

Figure 8 reveals that the impact of the two grouting techniques on lateral displacement is more pronounced in the inclinometer closer to the pile (CX1), compared to the farther one (CX3). The CX1 hole is positioned 2.75 m away from the 1# pile, while the CX3 hole is 4.3 m away. The maximum lateral displacement at CX1 is 2–3 mm, compared to 1 mm at CX3. This suggests that the influence of grouting decreases as the distance from the pile increases, aligning with findings from other studies [18,22,23]. The extent and intensity of jet grouting's impact on surrounding soil are influenced by factors such as grouting pressure, with typical influence zones ranging from 1 to 20 m and resulting displacements varying from millimeters to meters. In this study, the lateral effect is effectively localized, successfully achieving the intended objectives of disturbance control.

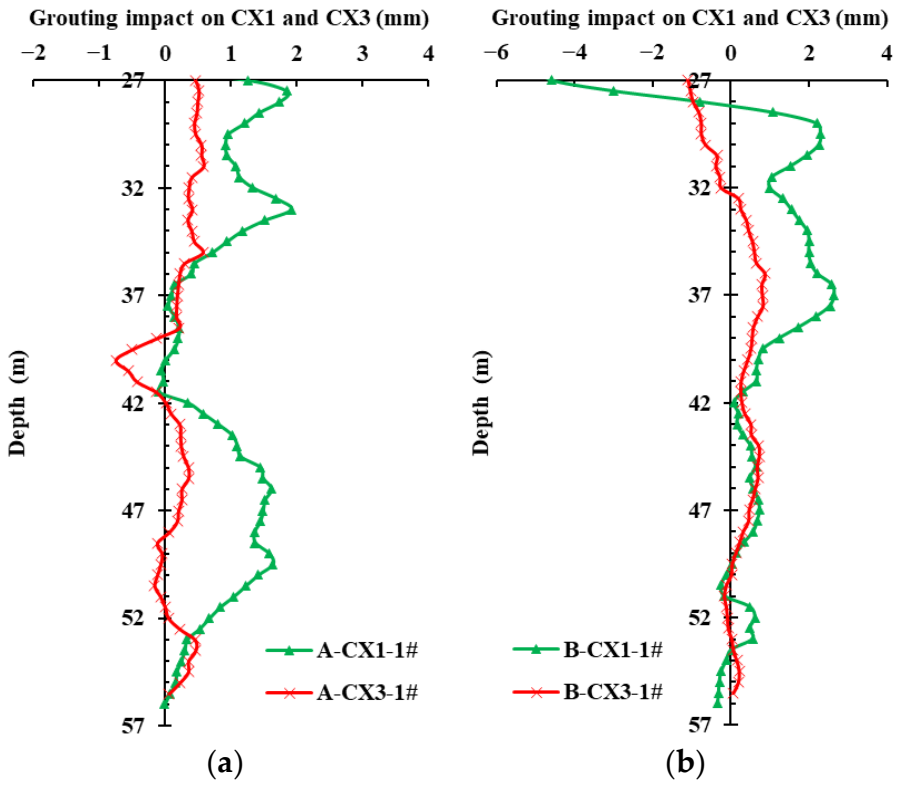


**Figure 8.** Analysis of grouting impact range for two techniques. (**a**) A-CX1-1# and A-CX3-1#. (**b**) B-CX1-1# and B-CX3-1#.

### *3.4. Impact of Different Stages*

In evaluating the impact of Pile 1# on CX1, monitoring data were assessed across three stages: pre-drilling (S1), grouting (S2), and after final stabilization (S3). As shown in Figure 9, the pre-drilling phase had a minimal impact on the adjacent soil, with an average lateral displacement of less than 1 mm. The grouting phase caused the most significant effect due to the increase in pore water pressure, resulting in noticeable outward soil movement, with a peak displacement of approximately 3 mm. The final stabilized displacement fell between the values observed in S1 and S2. As the excess pore water pressure dissipated and the soil consolidated, partial recovery of the displacement was observed. These observations indicate that while grouting initially causes significant soil movement, the effect lessens over time as the soil stabilizes and consolidation occurs.

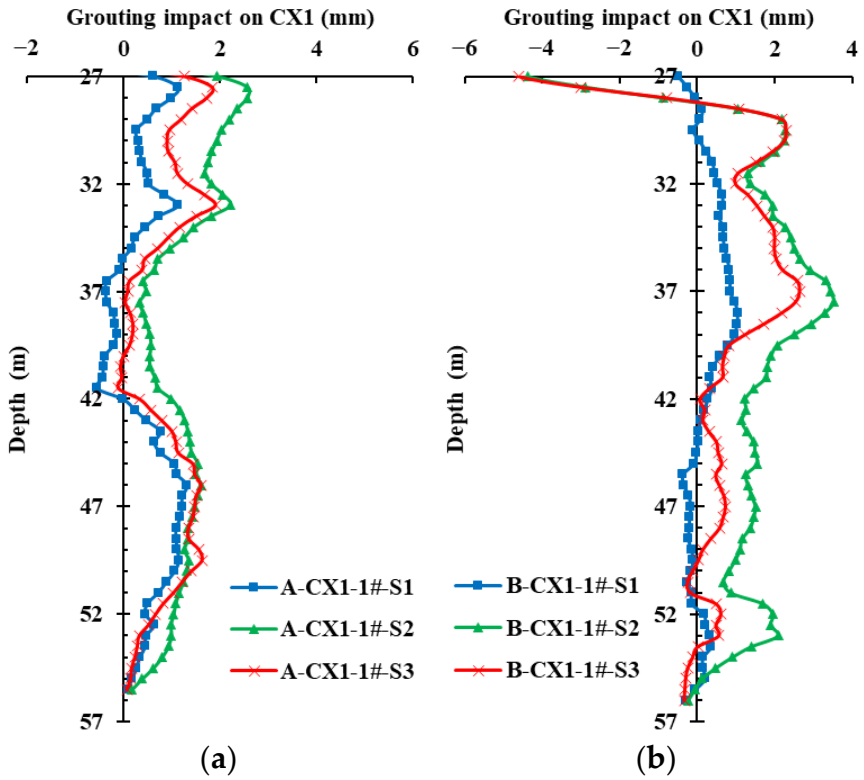


**Figure 9.** Analysis of the impact of two techniques on surrounding soil. (**a**) From A-CX1-1#-S1 to A-CX1-1#-S3. (**b**) From B-CX1-1#-S1 to B-CX1-1#-S3.

## 4. Impact on Adjacent Circular Diaphragm Walls

Piling, loading, and excavation can induce lateral displacement in surrounding soil, which subsequently applies lateral pressure on existing structures. In particular, during jet grouting, soil displacement may impose lateral pressures on adjacent diaphragm walls, posing a passive piles problem [26,28]. This lateral pressure on diaphragm walls is primarily due to soil movement rather than direct external forces and can be analyzed using methods developed for passive piles [30,33,41]. Figure 10 illustrates the approach used in this section, where soil displacements recorded by inclinometers during field tests are employed to predict the impact on diaphragm walls in the actual project.

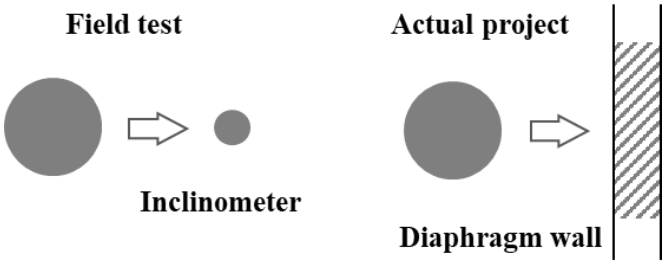


**Figure 10.** Impact of jet grouting on inclinometer and diaphragm wall.

### *4.1. Establishment of Theoretical Model*

Based on previous studies and engineering conditions, the basic assumptions for the forces acting on diaphragm walls are as follows:

1. The soil is assumed to be an equivalent homogeneous elastic body with a horizontal subgrade reaction modulus $k_h$;
2. The diaphragm walls are modeled as a unit-width plate (or rod) within a homogeneous and isotropic semi-infinite elastic body;

3. The axial force $N$ in the diaphragm walls is assumed to be constant with depth;
4. The sides of the wall are assumed to be smooth, and the influence of side friction is not considered.

Figure 11 illustrates the force equilibrium of a micro-segment within the diaphragm walls. Based on the force equilibrium $\sum F_y = 0$, the following equation can be obtained: $Q + q_{(z)} \cdot dz - (Q + dQ) = 0$; it can be rewritten as in Equation (1).

$$\frac{dQ}{dz} = q_{(z)} \tag{1}$$

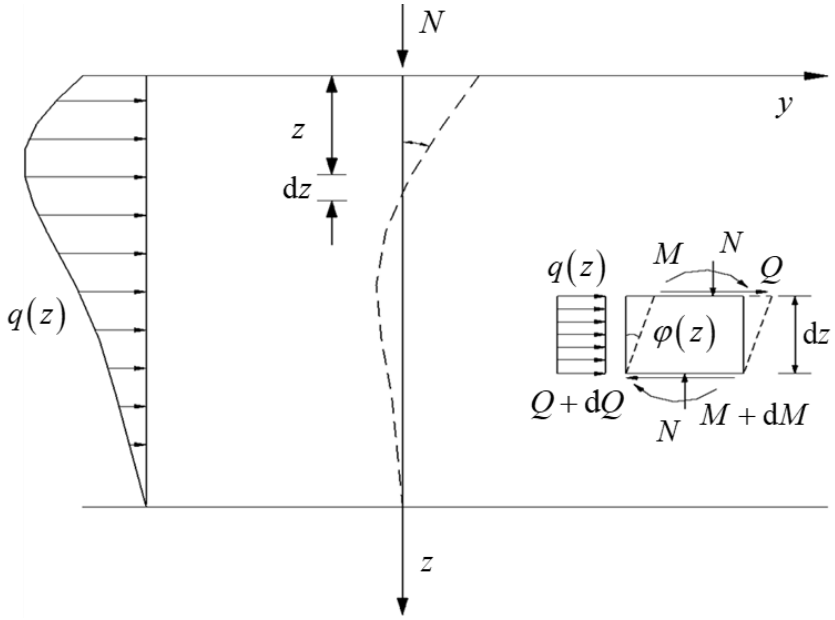


**Figure 11.** Force equilibrium of a micro-segment within the diaphragm wall.

Taking the moment at the center of the wall section yields the following equation, $M + Q \cdot dz - (M + dM) + N \cdot (-\varphi_z)dz + q_{(z)} \frac{(dz)^2}{2} = 0$. Neglecting the second-order high-order terms and differentiating yields

$$\frac{d^2 M_{(z)}}{dz^2} = \frac{dQ}{dz} - N\frac{d\varphi_{(z)}}{dz} \tag{2}$$

Combining Equation (1) and $\frac{dy}{dz} = \tan\varphi_{(z)} \approx \varphi_{(z)}$, $\frac{d^2y}{dz^2} = \frac{d\varphi_{(z)}}{dz} = \frac{M_{(z)}}{E_p I_p}$, the differential equilibrium equation for the internal forces of the wall is generated:

$$E_p I_p \frac{d^4 y}{dz^4} + N\frac{d^2 y}{dz^2} = q_{(z)} \tag{3}$$

where $z$ is the depth, positive downwards; $M_{(z)}$ is the bending moment, positive clockwise; $Q_{(z)}$ is the shear force, positive in the direction of the $y$-axis; $N$ is the axial force in the wall, positive in compression; $q_{(z)}$ is the lateral earth pressure, positive in the direction of the $y$-axis; $\varphi_{(z)}$ is the rotation angle, where a clockwise rotation of the wall results in $dz$ being positive and $dy$ being negative; $E_p$ is the elastic modulus of the diaphragm walls material, and $I_p$ is the moment of inertia of the wall section.

### *4.2. Horizontal Subgrade Reaction Modulus on the Wall*

During the jet grouting, the free displacement field of soil is denoted as $\delta$. Due to the stiffness of the wall, the combined displacement of the wall and soil is represented by $y$, where $0 < y < \delta$. The difference between these two is termed constrained displacement.

According to the Winkler hypothesis and based on the wall–soil deformation coordination condition, the lateral earth pressure $q_{(z)}$ per unit width on the wall, caused by the constraint, is

$$q_{(z)} = k_h(\delta - y) \tag{4}$$

Thus, the equilibrium differential Equation (3) can be written as

$$E_p I_p \frac{d^4y}{dz^4} + N\frac{d^2y}{dz^2} = k_h(\delta - y) \tag{5}$$

where $\delta$ is the free soil displacement adjacent to the jet grouting piles; the vertical axial force $N$ is considered as 0; and $k_h$ is the horizontal subgrade reaction modulus of the foundation soil, which can be determined using the $m$-method, expressed as $k_h = mz$, where $m$ is the proportional coefficient of the subgrade reaction modulus and can be selected according to relevant standard [42].

### *4.3. Numerical Solution of Equilibrium Differential Equation*

From Equation (5), it is evident that deriving an analytical expression for the pile displacement $y$ is quite challenging. This issue can be overcome by discretizing the equation using numerical methods. By performing numerical calculations, a series of discrete values for the pile displacement $y$ can be obtained, which can then be used to determine other parameters such as the internal forces of the pile. In this study, the finite difference method is employed to discretize the differential equation, and the corresponding results are obtained using MATLABR2024a.

As shown in Figure 12, the diaphragm walls are equally divided into $n$ sections along its depth, with each section having a length of $h$. From the top to the bottom of the pile are $y_0$, $y_1$, $y_2$, ……$y_n$, for a total of n points. For the n-th node, the second and fourth derivatives of $y_i$ are expressed as follows:

$$\begin{cases} \varphi_{(z)} = \frac{y_{i+1} - y_{i-1}}{2h} \\ M_{(z)} = EI\frac{y_{i+1} - 2y_i + y_{i-1}}{h^2} \\ Q_{(z)} = EI\frac{y_{i+2} - 2y_{i+1} + 2y_{i-1} + y_{i-2}}{h^2} \end{cases} \tag{6}$$

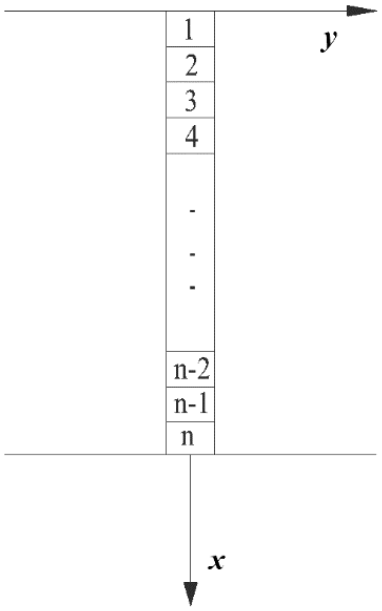


**Figure 12.** Micro-segment of the diaphragm walls.

Substituting Equation (6) into Equation (5) yields the discrete form of the equilibrium equation at $y_i$:

$$y_{i+2} + (a-4)y_{i+1} + (6+b-2a)y_i + (a-4)y_{i-1} + y_{i-2} = c\sigma \tag{7}$$

This can be briefly written as $A \times y = c\sigma$, where $a = \frac{Nh^2}{E_p I_p}$, $b = \frac{k_h \overline{B} h^4}{E_p I_p} = k_h c$, $c = \frac{\overline{B} h^4}{E_p I_p}$, $\sigma_{yz} = k_h \delta$, and $\overline{B}$ is the equivalent width of the pile.

According to Equation (7), $n-3$ equations can be generated, while there are $n+1$ unknowns. Therefore, additional boundary conditions are required. Generally, the top and bottom of the pile satisfy certain constraint conditions, which can be classified as free end, hinged end, and fixed end. In this study, the top and bottom of the diaphragm wall are assumed to be fixed, meaning both displacement and rotation are constrained to zero. This assumption is based on the presence of concrete pavement at the top and a dense soil layer at the bottom, which provide effective restraint to minimize movement at both ends.

$$\begin{cases} y_0 = 0 \\ y_n = 0 \\ y'_1 \approx \frac{y_1 - y_0}{h} = 0 \\ y'_n \approx \frac{y_n - y_{n-1}}{h} = 0 \end{cases} \tag{8}$$

Two virtual points are introduced at both the top and bottom of the pile, with their corresponding $y$ denoted as $y_{-2}$, $y_{-1}$, $y_{n+1}$, and $y_{n+2}$. There is a total of $n+5$ unknowns $y$. Equation (7) provides $n+1$ equilibrium equations. Combined with the boundary conditions determined by Equation (8), there are $n+5$ equations in total, matching the number of unknowns. The matrix form of coefficient $A$ is as follows:

$$\begin{bmatrix} 0 & 1 & 0 & -1 & 0 & & & & & & \\ 0 & 0 & 1 & 0 & 0 & & & & & & \\ 1 & a_0 & b_0 & a_0 & 1 & & & & & & \\ & 1 & a_0 & b_0 & a_0 & 1 & & & & & \\ & & & \cdot & \cdot & \cdot & \cdot & & & & \\ & & & & \cdot & \cdot & \cdot & \cdot & & & \\ & & & & & \cdot & \cdot & \cdot & \cdot & & \\ & & & & & 1 & a_0 & & a_0 & 1 & \\ & & & & & & 1 & a_0 & & a_0 & 1 \\ & & & & & & 0 & 0 & 1 & 0 & 1 \\ & & & & & & 0 & 1 & 0 & -1 & 0 \end{bmatrix} \tag{9}$$

where $a_0 = a - 4$, and $b_0 = 6 + b - 2a$.

By solving the equations, the lateral displacement $y_i$ at each node can be obtained, and subsequently, the corresponding rotation angle, bending moment, and shear force can be derived. The calculation formulas are as follows:

$$\begin{cases} \varphi_{(z)} = \frac{y_{i+1} - y_{i-1}}{2h} \\ M_{(z)} = EI \frac{y_{i+1} - 2y_i + y_{i-1}}{h^2} \\ Q_{(z)} = EI \frac{y_{i+2} - 2y_{i+1} + 2y_{i-1} + y_{i-2}}{h^2} \end{cases} \tag{10}$$

### *4.4. Analysis of Calculation Results*

Based on the results of the field experiments described in Section 3, the design plan employs the SJT technique to reinforce the soil from 22 to 50 m below the pit bottom. Using the theoretical derivation presented in this section, along with the free soil displacement data obtained from A-CX-1-5#, the lateral deflection and bending moment of the circular diaphragm wall induced by jet grouting were predicted (Figure 9). In the calculations, the diaphragm wall extends from a depth of 0.5 to 55.5 m, with a thickness of 1.5 m. According to the geotechnical investigation (Figure 2) and the recommended $m$ value for different soil

in relevant standards [42], the $m$ values are assigned as follows: 3000 kN/m$^4$ for 0–15 m, 5000 kN/m$^4$ for 15–24 m, 10,000 kN/m$^4$ for 24–47 m, 20,000 kN/m$^4$ for 47–62 m, and 25,000 kN/m$^4$ for 61–70 m. As shown in Figure 13, due to the disturbance caused by jet grouting, significant deflection occurs in the diaphragm wall between depths of 22 m and 50 m, with the predicted maximum lateral displacement reaching approximately 5 mm at a depth of around 25 m. The predicted bending moment of the diaphragm wall ranges from −1000 kN·m/m to 850 kN·m/m.

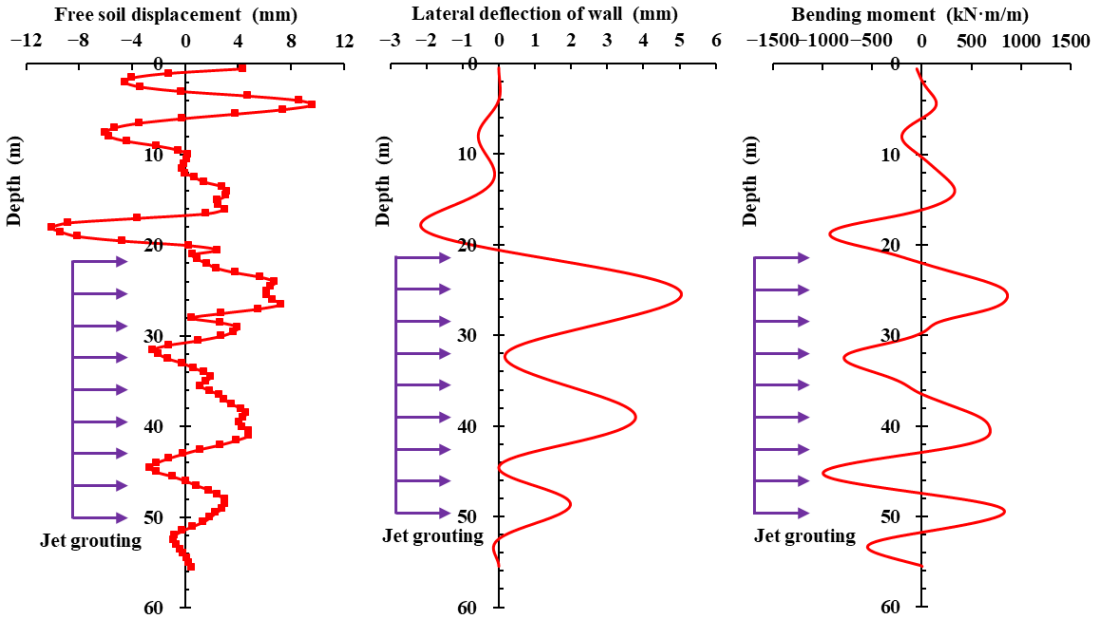


**Figure 13.** The predicted lateral effects of jet grouting include free soil displacement, deflection, and bending moment of diaphragm wall.

According to the monitoring scheme for the south anchorage of the North Channel Bridge, 64 steel stress monitoring sensors were installed on the diaphragm walls. The arrangement of these monitoring points is depicted in Figure 14. Using the tensile and compressive stress of the steel bars, along with the height of the concrete compression zone, the bending moment of the diaphragm wall at different heights can be estimated.

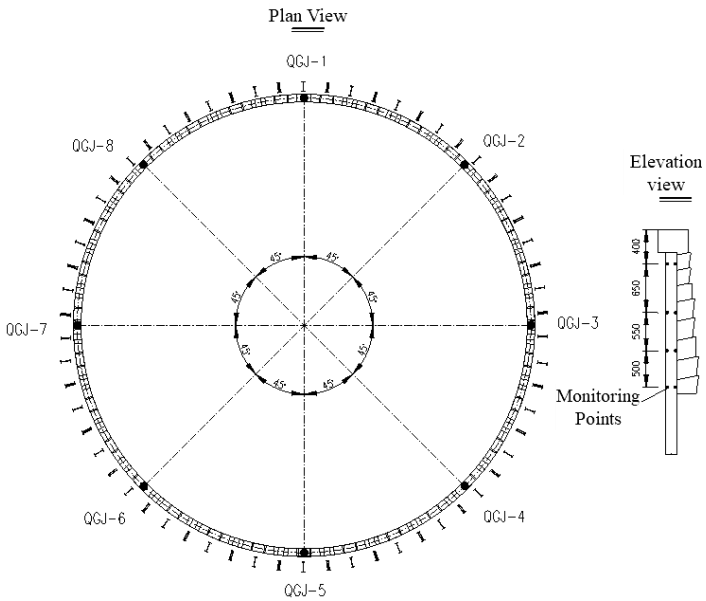


**Figure 14.** Layout of steel stress monitoring points on the diaphragm walls (cm).

Figure 15 illustrates the bending moment at measuring point QGJ-3 on the diaphragm wall. The black lines represent the predicted bending moments from Figure 13, while the other polylines represent the bending moments calculated from monitoring data at different times. The results show a consistent trend between the predicted and measured values, though the measured values are systematically higher. This discrepancy can be attributed to two main factors. First, the predictive model was based on displacement data from only five jet grout piles, whereas the actual project involved 2497 piles, leading to a cumulative lateral effect. Second, the inclinometers in the field test were positioned 1.5 m from the piles, whereas in the actual project, the piles were installed only 0.5 to 1.0 m from the diaphragm wall. This reduced distance intensified the observed disturbance, resulting in higher bending moments in the monitoring data.

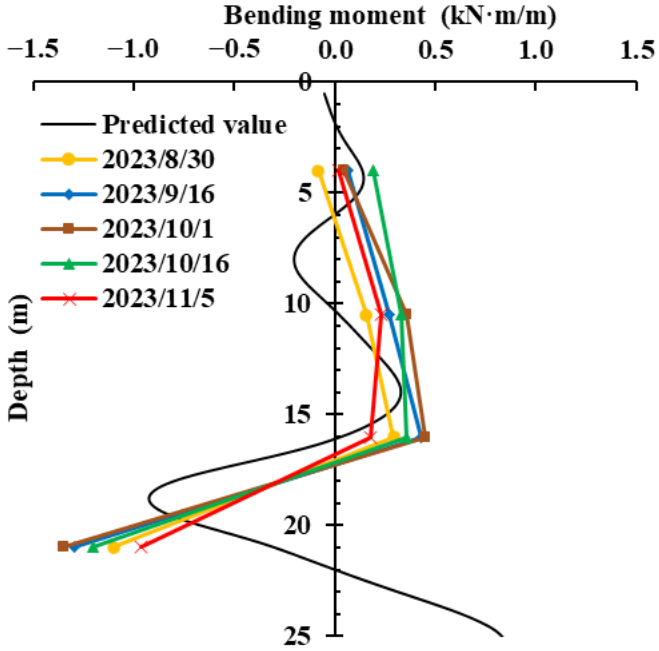


**Figure 15.** Bending moment in the diaphragm walls (kN·m/m).

## 5. Conclusions

This study provides valuable insights into the effects of high-pressure jet grout piles on surrounding soil and circular diaphragm walls, offering essential guidance for the design and construction of soil improvement projects. The main conclusions are as follows:

1. The influence patterns of jet grouting on surrounding soil were investigated, focusing on final lateral deformation, impact range, and different stages (pre-drilling, grouting, and stabilization). These findings enhance the understanding of lateral effects caused by jet grouting and provide essential data to support accurate assessments of ground deformation risks during the construction.
2. A comparative analysis shows that the Intelligent Sensing Super Jet Pile (SJT) technique causes less disturbance to surrounding soil than the Rodin Jet Pile (RJP) technique. The experimental results indicate that the SJT technique induces a maximum lateral displacement of approximately 6 mm at the closest inclinometer, with an influence range limited to around 4 m. The advantage of the SJT technique lies in its real-time monitoring and adaptive adjustment system, along with a larger pre-drilled hole, which effectively reduces lateral pressure on surrounding soil. For urban areas with strict deformation control requirements, the SJT technique is recommended, along with additional monitoring of soil and structural deformation.
3. This study presents a predictive method for assessing the impact of jet grouting on adjacent diaphragm walls, based on passive pile theory. Using soil displacement

data from field tests and the theoretical assumptions established in this research, the approach reliably predicts deformation and bending moments on nearby diaphragm walls. It provides a valuable reference for optimizing construction designs in similar projects.

4. For the circular diaphragm walls of the south anchorage of the North Channel Bridge, the SJT technique was employed for soil improvement. The predicted bending moments based on field test exhibited a consistent correlation with the measured data. However, the measured bending moments were generally higher than predicted, likely due to two main factors: the cumulative lateral effect from the significantly larger number of jet grout piles in the actual project, and the closer proximity of these piles to the diaphragm wall, which intensified the disturbance and resulted in higher bending moments.

Building on the findings of this study, future research could greatly benefit from advanced numerical simulation techniques to further clarify the impacts of jet grouting. Specifically, FEM models, potentially combined with PFC or DEM, could offer a highly detailed representation of the jet grouting process. Such simulations would enable the comprehensive analysis of the complex interactions between jet grout piles, surrounding soil, and adjacent structures, providing deeper insights into the lateral effects of jet grouting. Additionally, future studies could also explore different construction techniques and parameters to better understand their effects on soil and structural responses. This research would offer practical guidance for optimizing construction processes and fine-tuning jet grouting parameters to improve safety and efficiency in complex urban and geological environments.

**Author Contributions:** Methodology, X.S.; Software, Y.Y.; Investigation, Y.Y.; Resources, D.H.; Data curation, D.H.; Writing—original draft, Y.Y.; Writing—review & editing, X.S.; Supervision, X.S. All authors have read and agreed to the published version of the manuscript.

**Funding:** This research and the APC were funded by China Communications Construction Company Ltd. grant number YSZX-01-2021-01-B.

**Data Availability Statement:** The original data presented in this study are openly available in "Mendeley Data" at 10.17632/jh2r9rszw3.1.

**Conflicts of Interest:** Author Dongdong Han was employed by the company CCCC Highway Bridges National Engineering Research Center Co., Ltd. The remaining authors declare that the research was conducted in the absence of any commercial or financial relationships that could be construed as a potential conflict of interest.

## References

1. Broere, W. Urban underground space: Solving the problems of today's cities. *Tunn. Undergr. Space Technol.* **2016**, *55*, 245–248. [CrossRef]
2. Bobylev, N. Transitions to a high density urban underground space. *Procedia Eng.* **2016**, *165*, 184–192. [CrossRef]
3. Sadeghi, J.; Esmaeili, M.H. Safe distance of cultural and historical buildings from subway lines. *Soil Dyn. Earthq. Eng.* **2017**, *96*, 89–103. [CrossRef]
4. Sheng, E.S.Y.; Chuan, J.Y.T.; Ikhyung, H.K.; Osborne, N.H.; Boon, C.K.; Siew, R. Tunnelling undercrossing existing live MRT tunnels. *Tunn. Undergr. Space Technol.* **2016**, *57*, 241–256.
5. Eldukair, Z.A.; Ayyub, B.M. Analysis of recent US structural and construction failures. *J. Perform. Constr. Facil.* **1991**, *5*, 57–73. [CrossRef]
6. Sousa, R.L.; Einstein, H.H. Lessons from accidents during tunnel construction. *Tunn. Undergr. Space Technol.* **2021**, *113*, 103916. [CrossRef]
7. Zhang, H.; Shi, M.; Hu, W.; Jiang, Z. Analysis of sloping pier nearby embankment of overpass bridge in interchange. *J. Southeast Univ. Nat. Sci. Ed.* **2013**, *43*, 617–623.
8. Jerman, J.; Mašín, D. Evaluation of hypoplastic model for soft clays by modelling of Nicoll highway case history. *Comput. Geotech.* **2021**, *134*, 104053. [CrossRef]
9. Modoni, G.; Croce, P.; Mongiovì, L. Theoretical modelling of jet grouting. *Géotechnique* **2006**, *56*, 335–347. [CrossRef]
10. Wang, Z.F.; Shen, S.L.; Ho, C.E.; Kim, Y.H. Jet grouting practice: An overview. *Geotech. Eng. J. SEAGS AGSSEA* **2013**, *44*, 88–96.

11. Shibazaki, M. State of practice of jet grouting. In Proceedings of the International Conference on Grouting & Ground Treatment 2003, New Orleans, LA, USA, 10–12 February 2003; pp. 198–217.
12. Burke, G.K. Jet grouting systems: Advantages and disadvantages. In Proceedings of the GeoSupport 2004, Drilled Shafts, Micropiling, Deep Mixing, Remedial Methods, and Specialty Foundation Systems, Orlando, FL, USA, 29–31 January 2004; pp. 875–886.
13. Cheng, S.H.; Chao, K.C.; Wong, R.K.N.; Wang, W.I.M. Control of jet grouting process induced ground displacement in clayey soil. *Transp. Geotech.* **2023**, *40*, 100983. [CrossRef]
14. Wu, H.N.; Zhang, P.; Chen, R.P.; Lin, X.T.; Liu, Y. Ground response to horizontal spoil discharge jet grouting with impacts on the existing tunnels. *J. Geotech. Geoenvironmental Eng.* **2020**, *146*, 05020006. [CrossRef]
15. Wang, Z.F.; Shen, S.L.; Modoni, G.; Zhou, A. Excess pore water pressure caused by the installation of jet grouting columns in clay. *Comput. Geotech.* **2020**, *125*, 103667. [CrossRef]
16. Zheng, X.; Xu, Y.; Xu, Y.; Ao, J. Field-test investigation on influence of soft soil by continuous jet grouting. *Arab. J. Geosci.* **2022**, *15*, 1750. [CrossRef]
17. Lin, H.D.; Lin, S.C. Analysis of diaphragm wall displacement due to jet grouting in clay. *J. Geotech. Eng. Southeast Asia Geotech. Soc.* **2008**, *39*, 1–11.
18. Shen, S.L.; Wang, Z.F.; Cheng, W.C. Estimation of lateral displacement induced by jet grouting in clayey soils. *Géotechnique* **2017**, *67*, 621–630. [CrossRef]
19. Atangana Njock, P.G.; Zhang, N.; Zhou, A.; Shen, S. Evaluation of lateral displacement induced by jet grouting using improved random forest. *Geotech. Geol. Eng.* **2023**, *41*, 459–475. [CrossRef]
20. Shan, Y.; Luo, J.; Wang, B.; Zhou, S.; Zhang, B. Critical application zone of the jet grouting piles in the vicinity of existing high-speed railway bridge in deep soft soils with medium sensibility. *Soils Found.* **2024**, *64*, 101407. [CrossRef]
21. Fontanella, E.; Callisto, L.; Desideri, A. An interpretation of jet grouting effects on the retaining structures of a deep excavation and on adjacent buildings. In Proceedings of the Conference Geotechnical Aspects of Underground Construction in Soft Ground, Roma, Italy, 17–19 May 2011; pp. 941–948.
22. Wong, I.H.; Poh, T.Y. Effects of jet grouting on adjacent ground and structures. *J. Geotech. Geoenviron. Eng.* **2000**, *126*, 247–256. [CrossRef]
23. Feizi, S.; Nilsen, E.; Tsegaye, A.B.; Karlsrud, K.; Fornes, P.; Ritter, S. Effects of jet grouting on adjacent ground through numerical modelling. *Proc. Inst. Civ. Eng. Ground Improv.* **2024**, *177*, 357–369. [CrossRef]
24. Dong, Y.P.; Whittle, A.J. Effects of deep soil mixing and jet grouting on adjacent retaining walls and ground. In *Geotechnical Aspects of Underground Construction in Soft Ground*; CRC Press: Boca Raton, FL, USA, 2017; pp. 91–96.
25. Chai, J.; Carter, J.P.; Miura, N.; Zhu, H. Improved prediction of lateral deformations due to installation of soil-cement columns. *J. Geotech. Geoenvironmental Eng.* **2009**, *135*, 1836–1845. [CrossRef]
26. De Beer, E. The effects of horizontal loads on piles due to surcharge or seismic effects. In Proceedings of the Ninth International Conference on Soil Mechanics and Foundation Engineering, Tokyo, Japan, 10–15 July 1977.
27. Suleiman, M.T.; Ni, L.; Helm, J.D.; Raich, A. Soil-pile interaction for a small diameter pile embedded in granular soil subjected to passive loading. *J. Geotech. Geoenviron. Eng.* **2014**, *140*, 04014002. [CrossRef]
28. Ti, K.S.; Huat, B.B.K.; Noorzaei, J.; Jaafar, M.S. Modeling of Passive Piles-An Overview. *Electron. J. Geotech. Eng.* **2009**, *14*, 415–426.
29. Ni, L.; Suleiman, M.T.; Raich, A. Behavior and soil-structure interaction of pervious concrete ground-improvement piles under lateral loading. *J. Geotech. Geoenviron. Eng.* **2016**, *142*, 04015071. [CrossRef]
30. Bransby, M.F.; Springman, S. Selection of load-transfer functions for passive lateral loading of pile groups. *Comput. Geotech.* **1999**, *24*, 155–184. [CrossRef]
31. Karim, M.; Lo, S.-C.; Gnanendran, C. Behaviour of piles subjected to passive loading due to embankment construction. *Can. Geotech. J.* **2014**, *51*, 303–310. [CrossRef]
32. Yang, M.; Shangguan, S.; Li, W.; Zhu, B. Numerical study of consolidation effect on the response of passive piles adjacent to surcharge load. *Int. J. Geomech.* **2017**, *17*, 04017093. [CrossRef]
33. Radhima, J.; Kanellopoulos, K.; Gazetas, G. Static and dynamic lateral non-linear pile-soil-pile interaction. *Géotechnique* **2022**, *72*, 642–657. [CrossRef]
34. Jeong, S.; Seo, D.; Kim, Y. Numerical analysis of passive pile groups in offshore soft deposits. *Comput. Geotech.* **2009**, *36*, 1164–1175. [CrossRef]
35. Suleiman, M.T.; Ni, L.; Davis, C.; Lin, H.; Xiao, S. Installation effects of controlled modulus column ground improvement piles on surrounding soil. *J. Geotech. Geoenviron. Eng.* **2016**, *142*, 04015059. [CrossRef]
36. White, D.J.; Thompson, M.J.; Suleiman, M.T.; Schaefer, V.R. Behavior of slender piles subject to free-field lateral soil movement. *J. Geotech. Geoenviron. Eng.* **2008**, *134*, 428–436. [CrossRef]
37. Zhang, A.J.; Mo, H.H.; Zhu, Z.D.; Zhang, K.Y. Analytical solution to interaction between passive piles and soils. *Chin. J. Geotech. Eng.* **2011**, *33*, 120–127.
38. Hu, J.R.; Wang, J.C.; Zhu, X.R. Elastoplastic solution for interaction between slipping soil and adjacent piles. *Rock Soil Mech.* **2011**, *32*, 3414–3419, 3426.
39. Zhao, M.-H.; Liu, D.-P.; Zhang, L.; Jiang, C. 3D finite element analysis on pile-soil interaction of passive pile group. *J. Cent. South Univ. Technol.* **2008**, *15*, 75–80. [CrossRef]

40. Xiong, W.; Jiang, C.; Wang, T.; Wang, R.; Zhou, X. Safety-Margin Design for Gravity-Type Anchorage of Suspension Bridges over 2,000 m Long Based on Target Reliability. *J. Bridge Eng.* **2024**, *29*, 04024003. [CrossRef]
41. Hwang, R.N.; Lee, T.Y.; Chou, C.R.; Su, T.C. Evaluation of performance of diaphragm walls by wall deflection paths. *J. Geoengin.* **2012**, *7*, 1–12.
42. *JTG D63-2019*; Specifications for Design of Foundation of Highway Bridges and Culverts. Ministry of Transport of the People's Republic of China: Beijing, China, 2019.